ORCA – Online Research @ Cardiff

Mechanical response and predictive modelling of vascular self-healing cementitious materials using novel healing agents

Cristina De Nardi [*], Brubeck Lee Freeman, Diane Gardner, Tony Jefferson

Resilient Structures and Construction Materials (RESCOM) Research Group, School of Engineering, Cardiff University, Queen's Buildings, The Parade, Cardiff, CF243AA, Wales, United Kingdom

ARTICLE INFO

ABSTRACT

Self-healing systems represent an effective means of increasing the resilience of cementitious structures, extending service life and reducing cement production. This is achieved through the mitigation of cracking related durability problems. The success of a self-healing system is critically dependent on the selection of an appropriate healing agent, which depends upon the specific application, as well as a number of criteria including crack filling ability and the degree of mechanical healing required. In the present study, we develop modified formulations of a cyanoacrylate-based adhesive, suitable for use in a vascular self-healing cementitious material. The aim is to develop an 'ideal' healing agent for the self-healing system that has an extended shelf life and maximises load recovery. To this end, modified cyanoacrylates are tailored using a combination of predictive modelling and physical testing. The physical tests investigate both the mechanical, flow and chemical properties of the different healing agent formulations, including tensile strength, viscosity and curing. The predictive modelling employs a coupled chemo-mechanical model that is used to guide the physical testing programme through the prediction of the performance of different formulations. The results of the investigation show that a tailored formulation of a cyanoacrylate based healing agent increases the load recovery by 48% relative to the best performing original formulation. In addition, it is shown that the numerical model is able to predict the load response of new formulations with good accuracy.

1. Introduction

In recent decades, the design of vascular healing networks within concrete structures has attracted significant attention from the research community. Vascular networks can supply healing agent to damaged areas in a structure at discrete times or provide a continuous supply of agent if required. This makes them effective at responding to multiple damage events under real-world conditions [1]. The early design of vascular networks systems involved the embedment of glass tubes filled with cyanoacrylate [2]. Later, the influence of adhesive-filled glass tubes -acting as reservoirs within reinforced mortar beams-was studied by Joseph et al. [3], who confirmed the successful release of the healing agent and the enhancement of the post-healed beam properties for this healing system. Tsangouri et al. [4] studied the healing behaviour of hand-made clay tubes connected to an inlet–outlet supply system embedded in concrete slabs. Two liquids were flushed, i.e. a single component polyurethane (PU) healing agent and a solvent to clean the polymerised residuals from the channels. The study showed that

effective healing occurs locally with a consequent regain in mechanical properties [3]. Minnebo et al. [4] tested cementitious tubes equipped with four outlets and one inlet. The authors observed that whilst the PU prematurely reacted in the ceramic tubes, it remained active in the cementitious ones and was successfully distributed during damage, The system was able to repair mechanical damage from one and two loading cycles [4].

Despite their success in the laboratory, brittle vascular networks have had limited application in large scale structures due to their inherent fragility and the impact this has on the concrete manufacturing process [5]. Davies et al. [6] proposed a system of hollow channels to overcome some of the challenges related to brittle vascular networks. The authors employed a pressurised system to improve the distribution of the healing agents into the crack plane, with both sodium silicate (SS) and cyanoacrylate (CA) being explored. SS was found to be easier to handle and to supply into the vascular system, whereas CA provided greater strength recovery (up to 90%) in a relatively short period.

In recent years, there has been a focus on the fabrication of 2D and

---

3D vascular and mini-vascular 3D printed polymer networks, using Fused Deposition Modelling (FDM) technologies [7–9]. In addition to being fast, reliable and flexible, additive manufacturing offers the freedom to create vascular network healing systems of any shape and geometry [10].

A number of suitable healing agents for vascular networks have been studied. Mono or bi-component adhesives were tested, such as epoxy resins [10], polyurethane [9] and cyanoacrylates [11]. Generally, bi-component epoxy resins have limited potential due to the high polymerisation temperature required and low tolerance to wet conditions. Conversely, some mono-component agents have shown good chemical resistance [12]. Polyurethane foams can be used for cementitious self-healing vascular systems as well as for capsule-based systems with a proven capacity for repeated healing [4–13]. Cyanoacrylate-based adhesives (CA) have been used in the majority of self-healing investigations [14–16]. Their relatively good rheological and mechanical properties make them a suitable agent for self-healing concrete technologies. Several studies showed that during the healing process, the degree and rate of healing are dependent on the rate and size of the crack opening [17–19]. Previous investigations [20,21] have highlighted that since cured CA forms an increasing impermeable barrier to hydroxide ions, the rate of CA curing decreases over time. The authors also showed that CA's viscosity remains unchanged over a period of 15 min; however, the alkaline environment of the concrete matrix accelerates CA's polymerisation reactions, resulting in inadequate dispersion of the healing agent on the crack surface [22]. In an attempt to alleviate some of the problems with using CA as a healing agent in cementitious structures, De Nardi et al. [23] successfully explored ways of modifying CA such that it remained in a chemically stable liquid state for longer than standard CAs.

Significant advances have been made in both modelling [24] and experimental studies [25,26] There is now a range of approaches for simulating damage-healing behaviour, including continuum damage-healing mechanics [27,28], micromechanics [29], the discrete element method [30] and cohesive crack idealisations [31–33]. Alongside the development of damage-healing models, a number of researchers have developed models for the simulation of transport processes associated with self-healing at both the scale of a cementitious specimen (macroscale models) [34–37] and at lower scales (micro-/mesoscale models) [38,39]. To date, there are relatively few coupled models for simulating self-healing, though this state of affairs is changing and increasingly researchers are accounting for the various physico-chemical processes that govern the healing response in their models [40–45]. Among the first to do so was Hillouin et al. [45] who simulated autogenous healing of cracks using a version of CEMHYD3D (CemPP, a version of CemPy) for the healing reaction, which fed into a mechanical model (Cast3M) to study the associated regain in mechanical properties. Di Luzio et al. [40] coupled a hygro-thermo-chemical model to a solidification-microprestress-microplane model (M4), which they extended to account for healing, to simulate autogenous and stimulated healing in cementitious materials. Healing was simulated through a reaction affinity term, whilst a two-way coupling was considered between the transport and mechanical model components. Cibelli et al. [43] implemented the hygro-thermo-chemical model in a discrete setting, coupled to the lattice discrete particle model (Cusatis et al. [46]) to describe the mechanical behaviour. Framing the model in the discrete setting allowed the authors to represent concrete as a two-phase material at the meso-scale, comprising coarse aggregate and the cementitious matrix. Comparison of the model to experimental results showed that the model was able to reproduce the response with good accuracy.

As reported above, the authors of the current study have previously explored ways to improve the properties of CA as a healing agent in a vascular system [47]. However, one of the challenges that was not explored in this previous work is how to tune the properties of CA to a particular damage scenario for a specified structure subject to a given loading history. This problem is addressed in the work reported in this paper. The investigations described herein involved developing an analytical model to predict healing agent properties from the chemical components and then simulating the behaviour of a structure (or specimen) with an embedded vascular system using a coupled finite element model [33,36,44]. Specifically, the paper reports new results from a series of mechanical tests on autonomic self-healing in vascular networks samples using different formulations containing 2-ethyl cyanoacrylate (CA) - a commercial monomer - acrylic acid (AA) and nitroanthraquinone (nAq). The trialled modified CA (n-CAs) mixes contain components CA, AA and nAq in different ratios (CA:AA: nAq). In addition to this, results on flow and physicochemical properties are reported, building on those presented previously [23]. The combined experimental and numerical investigation also developed a series of design curves to help engineers select a suitable healing agent and predict its properties.

The structure of the remainder of this paper is as follows.

- Section 2 describes the experimental programme, gives details of the experimental procedures and describes the testing arrangements on both the n-CAs and on the vascular network system within concrete samples.
- Section 3 presents the coupled finite element chemo-mechanical model used for the predictive simulations.
- Section 4 presents the experimental results, development of the predictive functions for n-CA properties, the model predictions and design curves, along with some discussion.
- Section 5 draws conclusions from the study.

2. Experimental materials and methods

The experimental programme focusses on the flexural behaviour of a vascular self-healing system, which has healing-agent supply channels embedded in concrete prisms as reported by [6,18,47].

Innovative (tailored) formulations of cyanoacrylates (n-CAs) were prepared by mixing a commercial 2-ethyl cyanoacrylate (CA) with acrylic acid (AA) and nitro-anthraquinone (nAq). The components CA: AA:nAq varied in the ratios 3–1:1:0.02. The n-CA's polymerisation rate was evaluated at 21 days – assuming that this provided a sufficient curing time - via a pull-off test. In addition, the degree of wetting was evaluated using contact angle measurements. More details on the pull-off test and measurement the contact angle can be found in [23]. Finally, rheological measurements were carried out by using a Paar MCR 102 rheometer, equipped with a dual concentric cylinder systems (DIN EN ISO 3219 and DIN 53019).

2.1. n-CAs property assessment

The various test series undertaken are summarised below.

i) Cement mortar specimens were cast and subsequently bonded together with n-CA, then tested via a tensile (pull-off) test at 21 days to evaluate the maximum bond strength of the trialled n-CA formulations, details of the test set up can be found in [23].

ii) The contact angle (θ_c) of the n-CA formulations with cementitious substrates was examined via the sessile drop technique. The substrate was the open cast face of a cement mortar cube manufactured for the pull-off test [23].

iii) The flow characteristics of the n-CA formulations were measured by using small samples, for a range of CA:AA ratios (0.5:1); it was assumed that the influence of the nAq (2% volume) was here negligible. Pure CA monomers cure so quickly that formulations with a CA: AA ratio larger than 0.5:1 could not be reliably measured for viscosity. For these reasons the viscosity in the whole range has been obtained by fitting the Grunberg and

Nissan relationship [48] (Equation (1)) on data measured from 0 to 0.5 of volumetric fraction.

$$ln(\eta) = \varphi_{CA} \, ln\left(\eta_{CA}^0\right) + \varphi_{AA} \, ln\left(\eta_{AA}^0\right) + b\varphi_{CA}\varphi_{AA} \tag{1}$$

where η is the kinematic viscosity of the mixture; η_{CA}^0 and η_{AA}^0 are the kinematic viscosities of the pure cyanoacrylate adhesive and acrylic acid respectively; φ_{CA} and φ_{AA} are their volumetric fractions; and b is a co-efficient calculated by data regression.

2.2. Vascular system and materials

The method used to form the embedded networks in the current experiments follows a procedure developed by Davies et al. [17,18,49]. This procedure involves casting 4 mm diameter polyurethane tere-phthalate (PET) tubes into the prismatic concrete samples and subsequently removing them after 24 h of concrete curing.

The twin moulds for the prismatic samples (see Fig. 1) had four pre-drilled holes in each stop-end. The 4 mm PET tubes were lightly tensioned by hand and secured with crocodile clips on the stop-end external faces (see Fig. 1). The moulds were lightly coated with oil to facilitate demoulding. When hosting CA within the channels, the system has already been shown to have significant healing performance in relatively short time periods [50] and has been tested successfully in a full-scale application [49]. More details of the system can be found in Selvarajoo et al. [18].

The n-CA formulations were introduced into the vascular channels via syringe and the channels were then pressurised using a pressurised airline, connected to a regulator (SMC IR3000-03BG-R) via a 6 mm PET tube. The flexible tubes were attached to an inlet manifold with multiple outlets to tee connectors which were then fastened to the PET supply tubes of the specimen, as shown in Fig. 2. The supply pressure was fixed at 0.3 bar, since this was found to be the optimum delivery pressure for the system tested [18]. The pressure was applied to all supply tubes at one end of the specimen. At the opposing end of the specimen, each of the PET supply tubes was individually locked off using a plastic clamp once the channel was full.

2.3. Concrete and curing procedure

The mix constituents and proportions of the concrete comprised: Ordinary Portland Cement, CEM II/A-L 32,5 R (562 kg/m^3); 0–2 mm dried fine aggregate sand (562 kg/m^3); 0–10 mm crushed limestone coarse aggregate (1124 kg/m^3); and water (253 kg/m^3). The same mix proportions, constituents and mixing protocol were used to form all cementitious specimens. The dry materials (coarse aggregate, fine sand, cement) were mixed for 30 s, at which point all of the water was added while the mixer was rotating; the mixing was stopped after a total of 240 s. The moulds were filled in 3 layers, with the initial 10 mm thick layer providing a bed for the PET channels. Each sample was vibrated for 30 s
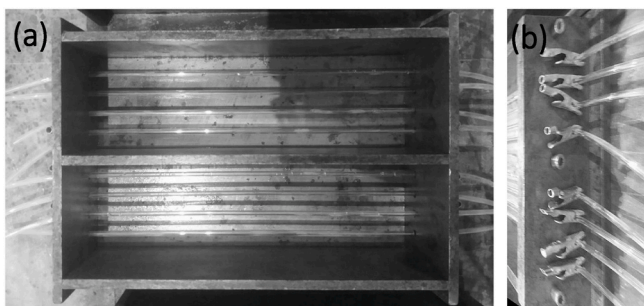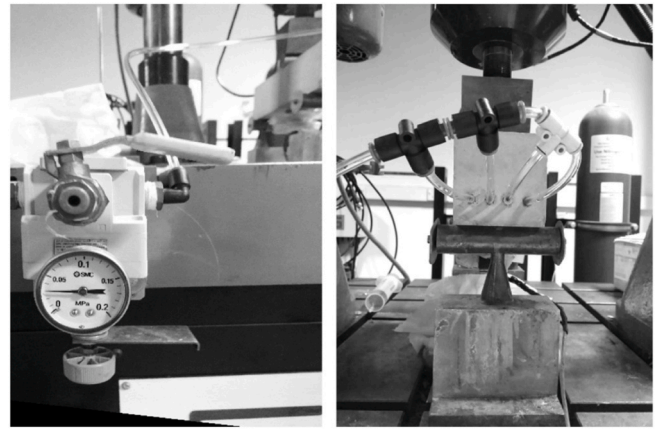

Fig. 2. Pressure gauge and pressurised airline.

to a maximum of 45 Hz. All specimens were cast, demoulded after one day and then immersed in a water tank (20 °C ± 5 °C) for four days. It is noted that prior to immersion in the water tank, the PET tubes were removed. After this time, a 5 mm central notch was created on the lower surface using a diamond blade masonry table saw (Controls Cernusco model 55-CO210/D) in order to induce a single vertical crack during the 3-point bending testing stage. Samples were then placed in the oven at 60 °C for two days and then allowed to cool at room temperature in the desiccator for one further day prior to testing. Since CA is highly sensitive to moisture, which accelerates the polymerisation process [51], the drying process in the oven is needed to remove most of the capillary water; it being reasonably assumed that the temperature of 60 °C causes no thermal shock to the cementitious matrix [52].

The channels ends were then enlarged to a diameter of 6 mm for a depth of 10 mm to host a set of 100 mm long PET supply tubes (outer diameter of 6 mm and an inner diameter of 4 mm) that were glued into position using commercially available CA. Steel knife edges were then bonded to the underside of the specimen either side of the notch to accommodate a Crack Mouth Opening Displacement (CMOD) clip gauge.

2.4. Experimental arrangement

After the drying procedure, prisms were loaded until failure (control series) or until a prescribed CMOD equal to 0.3 mm was recorded, using a 3-point bending test in accordance with BS EN 12390–5 [53], followed by unloading. The 0.3 mm CMOD was chosen as a typical serviceability crack width, according to EN 1992-1-1 [54]. A CMOD rate equal to 0.0001 mm/s, was used throughout the test.

The vascular network system and flexural test arrangement are illustrated in Fig. 3. The three-stage testing procedure is as follows.

- Stage 1: the samples are loaded until the CMOD reaches 0.3 mm, or until failure in the control tests):
- Stage 2: samples are placed in laboratory environmental conditions (20° ± 5, RH ∼ 45%) for 1 day in the case of standard CA and for 21 days for the n-CAs:
- Stage 3: the samples are reloaded until failure.

2.5. Experimental programme

The experimental programme, as presented in Table 1, is separated into 2 main groups. The aim of Group_1 was to evaluate the mechanical chemical and physical properties of the new n-CA formulations by means of pull-off, contact angle and viscosity experiments described above.

The aim of Group_2 was to explore the interaction between cracking

Fig. 1. Moulds for prismatic specimens, showing PET tubes used to form flow channels (a), crocodile clips on the mould side to keep the PET tubes in the position (b).
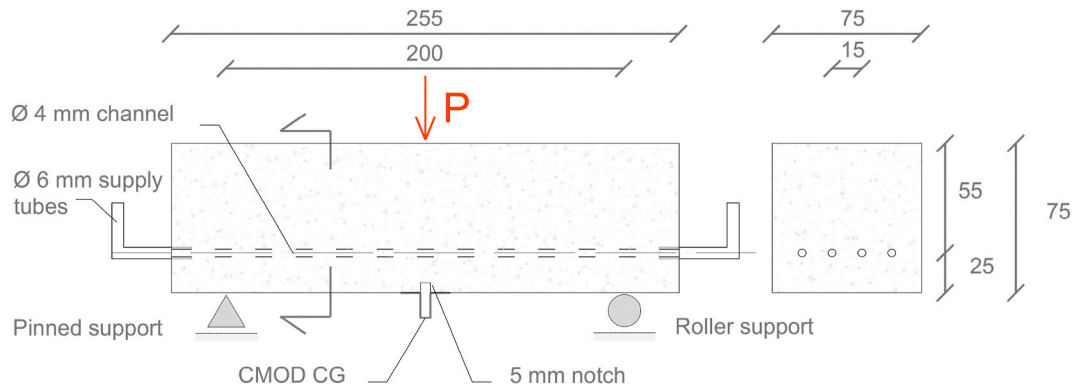
Fig. 3. Vascular network system and flexural test arrangement.

Table 1
Details of the experimental programme, sample designations and number of samples per test.

Sample Designation	Ratio CA:AA: nAQ	GROUP_1 No. Specimens			GROUP_2 No. Specimens
		TENSILE TEST (PULL-OFF) @ 21 curing days	CONTACT ANGLE	VISCOSITY	3 POINT-BEND TESTS
Pure CA (Control)	1:0:0	3[a]	3[a]	1	3
3:1	3:1:0.02	3	3	1	3
2:1	2:1:0.02	3[a]	3[a]	1	3
1:1	1:1:0.02	3[a]	3[a]	1	3

[a] Results are reported in [23].

and healing for CMOD equal to 0.3 mm and healing-agent (n-CA) supply scenarios.

3. Numerical model

The numerical model employed is a coupled chemo-mechanical finite element model. The mechanical component uses a damage-healing cohesive zone model [44] that is implemented into an embedded strong discontinuity element [33]. The mechanical model allows for overlapping damage-healing processes and an arbitrary number of damage-healing events. The transport component of the model couples Richard's equation for describing flow in the cementitious matrix to the Navier-Stokes equations for describing flow in discrete cracks [36]. The coupled finite element model is described in detail in [33,36,44]. Here we provide an overview of the main components.

3.1. Mechanical model

The mechanical component is described by a damage-healing cohesive zone model that relates the tractions (τ_{cp}) across a crack plane to the crack opening displacements (**d**):

$$\tau_{cp} = (1 - \omega) \cdot \mathbf{K} : \mathbf{d} + h \cdot \mathbf{K} : (\mathbf{d} - \mathbf{d}_h) \tag{2}$$

where **K** is the elastic stiffness, h is the degree of healing, $\mathbf{d}_h$ is the relative displacement at the time of healing and ω is the damage variable that is governed by an exponential softening function [33]:

$$\omega = 1 - \frac{d_t}{\zeta} e^{-c1 \frac{\zeta - d_t}{d_m - d_t}} \tag{3}$$

in which $d_t = f_t h_{cp}/E$, where f_t is the tensile strength of the material, E is Young's modulus and h_{cp} is the assumed thickness of the crack plane (taken as 10 mm). $c_1 = 5$ is a softening constant, d_m is the relative displacement at the end of the softening curve and ζ is the damage evolution parameter that depends on the maximum value of the inelastic relative displacements.

The degree of healing is given by the degree of cure of the healing agent at the centre of the crack [44]:

$$h(w_c, t) = \Phi\left(\frac{w_c}{2}, t\right) \tag{4}$$

where w_c is the crack width, t is time and $\Phi(x, t)$ is the function giving the degree of cure profile to be introduced in section 3.3. For a complete description of how healing variables are updated and how an arbitrary number of damage-healing events are accounted for the interested reader is referred to [44].

3.2. Transport model

3.2.1. Matrix flow

The matrix flow component is described by Richard's equation and employs Darcy's law for the liquid flux:

$$\frac{\partial(\rho n S)}{\partial t} + \nabla \cdot \left(-\rho \frac{K_{mi} K_r(S)}{\mu} (\nabla P_h - \rho \mathbf{g}) \right) + Q_{mtx} = 0 \tag{5}$$

where ρ is the healing agent density, n is the porosity, S is the degree of saturation, K_{mi} is the intrinsic permeability of the medium, μ is the dynamic viscosity, $\mathbf{g}$ is the gravitational vector, P_h is the healing agent pressure and K_r is the relative permeability that depends on the degree of saturation according to:

$$K_r(S) = S^\lambda \left(1 - \left(1 - S^{\frac{1}{m}} \right)^m \right)^2 \tag{6}$$

where λ accounts for the connectivity and tortuosity of the pores.

The degree of saturation is related to the capillary pressure, P_c, through the moisture retention curve that reads:

$$P_c(S) = a\left(S^{-\frac{1}{m}} - 1 \right)^{1-m} \tag{7}$$

where a and m are constants that depend on the medium and $P_c = P_g - P_h$, where P_g is the gas pressure.

The source sink term (Q_{mtx}) represents the transfer of fluid between the matrix and the cracks and is described using an embedded discrete fracture approach [55]:

$$Q_{mtx} = \frac{2n}{\mu h} \frac{K_{mi} K_c}{K_{mi} + K_c} (P_h - P_{hcrk}) \tag{8}$$

where P_{hcrk} is the healing agent pressure in the crack, $K_c = w_c^2/12$ is the crack permeability, h is a measure of the element size and the factor 2 is included to account for flow through both crack faces.

3.2.2. Crack plane flow

The crack plane flow component is described by the Navier-Stokes equations of mass and momentum balance:

$$\frac{\partial(\rho u)}{\partial t} + u\nabla(\rho u) = -\nabla P_{hcrk} - \psi u - u Q_{mtx} + \rho g \sin(\vartheta) \tag{9}$$

$$\frac{\partial(\rho w_c)}{\partial t} + \nabla(\rho w_c u) - w_c Q_{mtx} = 0 \tag{10}$$

where u is the healing agent velocity, ϑ is the inclination of the crack and ψ is the viscous resistance to flow that is given as:

$$\psi = \frac{\mu}{K_c + 0.5\mu w_c \beta_w \beta_{wr}} \tag{11}$$

where β_w is a factor to allow for wall slip and $\beta_{wr}(\varphi)$ is the relative wall slip factor that reduces wall slip with curing of the healing agent.

The driving pressure for flow in the crack plane comprises applied pressure and capillary pressure that is given by the Young-Laplace equation:

$$P_c = \frac{2\gamma \cos(\theta_d)}{w_c} \tag{12}$$

where γ is the healing agent surface tension and θ_d is the dynamic contact angle that is a function of the static contact angle (θ) and the healing agent velocity:

$$\tanh(c_{a1}(u\mu/\gamma)^{c_{a2}}) = \frac{\cos(\theta_s) - \cos(\theta_d)}{\cos(\theta_s) + 1} \tag{13}$$

where c_{a1} and c_{a2} are constants.

3.3. Chemical model

The chemical component simulates the curing of cyanoacrylate as a diffuse reaction front that propagates from the crack faces, described by:

$$\Phi(x,t) = \frac{1}{2}\left(1 - \tanh\left(\left(\frac{2}{\sqrt{\pi}}\right)\left(\frac{x - z(t) - z_c}{z_c + \sqrt{\frac{z(t)}{z_{c1}}}}\right)\right)\right) \tag{14}$$

where x denotes the position measured from the crack face, z_c is a wall factor, z_{c1} is a diffusion coefficient and $z(t)$ is the position of the reaction front, the propagation of which is described by:

$$z(t) = z_{c0}\left(1 - e^{-\frac{t}{\tau}}\right) \tag{15}$$

where z_{c0} is a critical curing depth and τ is the healing time parameter.

Finally, the effect of curing on the viscosity of the healing agent is described by a chemo-rheological model [56]:

$$\mu = \mu_i \left(\frac{\Phi_g}{\Phi_g - \Phi}\right)^{nv} \tag{16}$$

where μ_i is the initial viscosity, nv is an exponent, Φ_g is the degree of cure at the gel point at which a rapid increase in viscosity is observed and Φ is overall degree of cure across the width of the crack.

3.4. Relationship between healing indices and the healing parameters

Healing efficiencies can be calculated by the comparing pre-cracking and post-healing responses with those of the control specimens. The nominal flexural stress is calculated using Equation (17):

$$\sigma^k = \frac{3Pl}{2b\,d^2} \tag{17}$$

where P is the peak load, l is the span (200 mm), b is the width of the concrete samples (75 mm) and d is the depth (75 mm).

As indicated by Homma et al. [57], and commonly adopted by other investigators [8,58], the healing (or recovery) index can be calculated using the following equation:

$$\chi_\sigma^k = \frac{\overline{\sigma}_{healed}^k - \overline{\sigma}_{damaged}^k}{\overline{\sigma}_{undamaged}^k - \overline{\sigma}_{damaged}^k} \tag{18}$$

In which the average of the flexural strengths are defined in Fig. 4 and it is noted that $\overline{\sigma}_{healed}^k$ indicates the strength gained after the healing period, $\overline{\sigma}_{damaged}^k$ is the residual strength measured at the prescribed pre-cracked opening, and $\overline{\sigma}_{undamaged}^k$ is the maximum stress exhibited by the same specimens in undamaged conditions.

With reference to the notation in Fig. 4, the index of stiffness recovery χ_E^k (%) is defined as follows:

$$\chi_E^k = \frac{\overline{K}_{healed}^k - \overline{K}_{damaged}^k}{\overline{K}_{undamaged}^k - \overline{K}_{damaged}^k} \tag{19}$$

4. Results and discussion

4.1. Group 1 results

The average bond strengths of the mortar cubes tested at 21 days, calculated from the maximum force during the tension test, are summarised in Table 2. The contact angle reported for cement mortar substrates, calculated as the average contact angle of the three drops on that substrate, is also provided in Table 2 along with the coefficients of variation (CoV %). In the same table, the viscosity of the n-CA formulations is reported.

As revealed in a previous study [45], the addition of AA to the commercial CA retards the polymerisation reaction. This highlights the potential to limit pre-mature polymerisation, avoiding blockage of the vascular network and thus allowing the system to heal multiple occurrences of damage.

As expected, all of the n-CA formulations exhibited a significant decrease in bond strength with respect to the pure commercial CA; nevertheless, the best case (3:1) exhibit a bond strength value of the same order of magnitude of concrete tensile strength reported in Table 5. The wettability with respect to the cementitious substrate increased in proportion to ratio of AA in the formulation. Similarly, as the ratio of AA
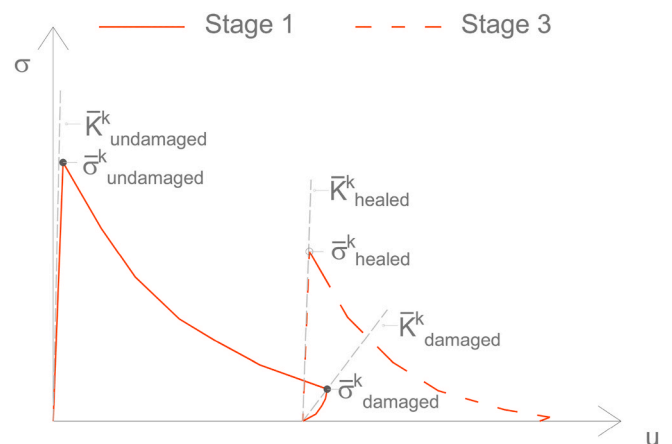

Fig. 4. Typical damage -healing response in flexural: notation and definition of the parameters for the indices of healing.

Table 2
Pull off test results, contact angle results and viscosity measurements for varying n-CA formulations.

Designation n-CA formulations	Bond strength (N/mm^2)	Contact angle θ_c (degrees) (CoV %)	Viscosity (Ns/m^2)
CA	2.7 (17)[a]	26 (18)	0.1[b]
3:1	1.2 (28)	11 (6)	0.071
2:1	1.0 (72)	11 (6)	0.059
1:1	0.7 (38)	6 (38)	0.031

[a] Tests failed in the concrete sample at the level of the bolt head.
[b] Value reported in the datasheet.

in the formulation decreased so did the viscosity of the n-CAs, this suggests shorter fixture times [59].

4.2. Group 2 results

Table 3 reports the average of nominally identical specimens filled with different n-CA formulations and tested in flexure until a CMOD equal to 0.3 mm was reached. The indices of strength and stiffness recovery are also summarised in Table 3. The Table includes the results of a 3:1 formulation, which was determined using a tailoring exercise that is described in the next section of this paper.

The results presented in Table 3 show that the greatest strength and stiffness recoveries were measured in the samples with the 3:1 CA formulation, which significantly out-performed the commercial CA. As expected, the system filled with the 1:1 formulation exhibited the lowest healing performance; however, in this case the healing time of 21 days was insufficient for a complete polymerisation reaction [45], and thus inadequate bonding of the crack surfaces was achieved.

4.3. Flexural test on concrete samples containing vascular networks and model calibration

In this section, the load-CMOD response curves of the three-point bending samples with embedded vascular networks are presented. In addition, a calibration exercise was undertaken to determine relevant model parameters. In the numerical simulations, differences in healing agent properties are accounted for through material parameters such as viscosity and contact angle, whilst differences in bond strength are assumed to arise solely from differences in the degree of curing, as described by the healing time parameter, τ. It is noted that in this section, the results of the 3:1 formulation are not presented as they were not part of the initial testing, nor were they used for model calibration. Once the model was calibrated, predictive simulations were undertaken to identify the 'ideal' healing agent. The 3:1 formulation resulted from predictive simulations undertaken to identify the 'ideal' healing agent. Following the predictive simulations, the identified 'ideal' 3:1 formulation was prepared and physically tested to assess the accuracy of the model predictions. The results for the 3:1 formulation can be seen in Section 4.5.

The results of the physical tests and calibrated numerical simulations can be seen in Fig. 5 for a typical stage 1 response for a CMOD of 0.3 mm, and in Fig. 6 for the stage 3 response of the CA, 1:1 and 2:1 formulations. It is noted that the stage 1 loading takes place pre-healing and as such

Table 3
Flexural test results and indices of healing for one cycle of damage-healing.

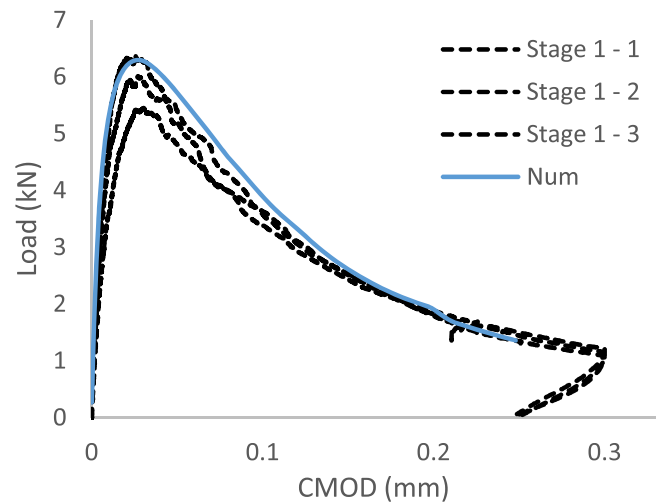| Group_2	$\sigma_{undamaged}^{k\,1}$ N/mm^2 (CoV%)	$\sigma_{damaged}^{k\,1}$ N/mm^2 (CoV%)	Healing		
			$\sigma_{healed}^{k\,14}$ N/mm^2 (CoV%)	χ_σ^k	χ_E^k
2_CA	4.11 (3)	1.04 (10)	2.45 (10)	46%	54%
2_3:1	3.77 (8)	0.83 (34)	2.90 (8)	70%	75%
2_2:1	4.23 (6)	0.82 (5)	1.57 (22)	22%	66%
2_1:1	4.12 (2)	0.58 (20)	0.53 (12)	0	39%

Fig. 5. Mechanical response of stage 1.

the healing agent is assumed to have negligible impact on the response. It is noted that the numerical model does not capture the full loading-unloading response as it does not include rough crack contact. As a result of this, the model will predict unloading to a CMOD of zero, which is not in line with the experimental results.

It can be seen from Fig. 5 that the stage 1 response shows the typical exponential-type softening behaviour associated with plain concrete, and that the numerical simulations match this response with good accuracy. The stage 3 softening responses (Fig. 6) of all of the self-healing specimens exhibit similar characteristic behaviour to the control specimens. The key difference between the responses of specimens with different healing agents lies in the stage 3 peak loads, which range from approximately 4 kN for the commercial CA, to no stage 3 peak for the 1:1 formulation. It is thought that this difference in strength arises from differences in the degree of cure of each of the healing agents after the healing period, though we note that there may also be differences in the bond strength of fully cured materials.

The numerical simulations provide a good match to the stage 3 experimental responses, including the post-healed peak load and the softening behaviour. The largest discrepancy can be seen in the 1:1 formulation. The numerical results for the 1:1 formulation follow the line of continuing damage of the virgin concrete (i.e. the healing agent has no discernible effect), whilst the experimental results show a drop in residual strength upon reloading. In this case, it is thought that the sample continued to undergo some damage following unloading, leading to a lower residual strength of the material. The numerical model does not account for this and as such, the residual strength is that of the sample at the point of unloading.

In addition to being able to reproduce experimental results, the numerical simulation can also be used to gain insight into other aspects of the response. In particular, the model was used to predict the quantities of healing agent used in each test, as this is an important quantity when using capsule or vascular based healing systems. The mass of healing agent in the crack plane (M_{cp}) was calculated as:

$$M_{cp} = \rho \int_{c_h} w_c t_h \tag{20}$$

in which c_h is the predicted healing agent rise height in the crack and t_h is the out of plane thickness of the specimen.

The mass of healing agent in the cementitious matrix (M_m) was obtained as:

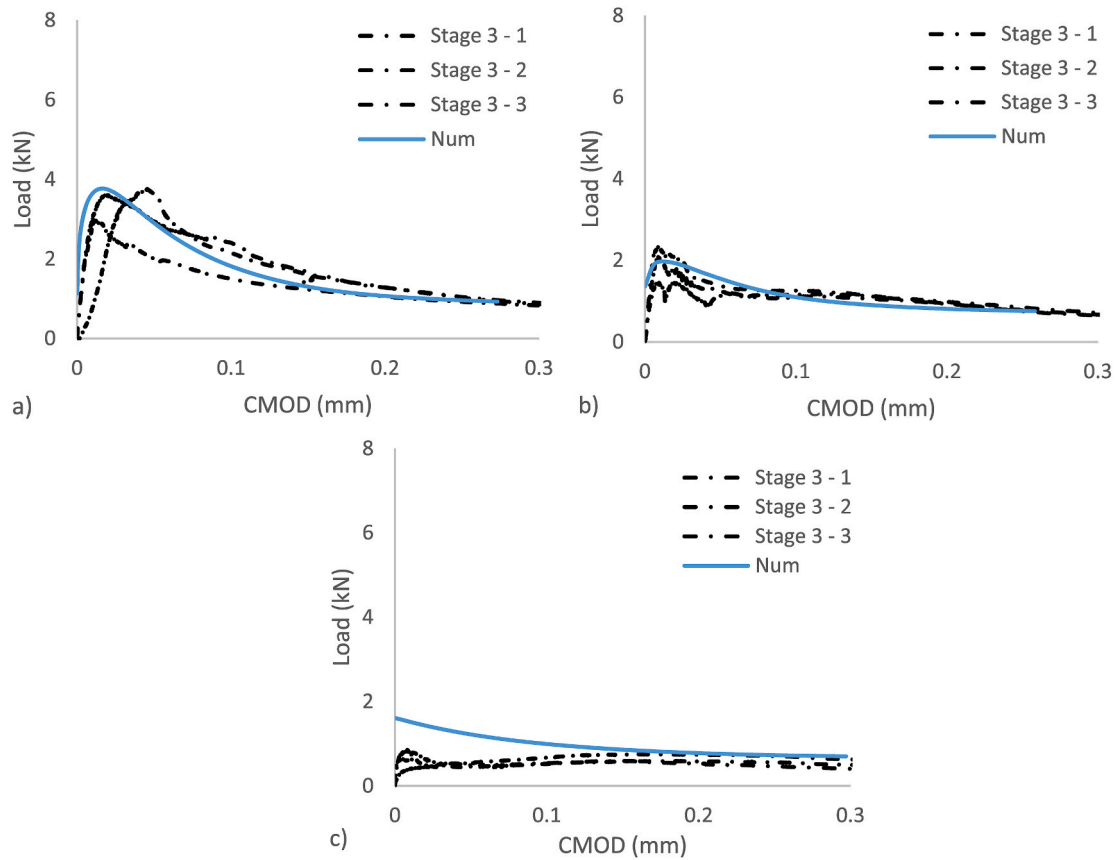$$M_m = \rho n \int_{\Omega_m} S t_h \tag{21}$$

Fig. 6. Mechanical response of stage 3 specimens top a) CA, b) 2:1 and c) 1:1.

in which Ω_m is the matrix domain.

These quantities can be seen in Table 4, wherein much higher total quantities of the 2:1 and 1:1 formulations are required than that of the commercial CA. The quantities of healing agent in the crack are similar, whilst there are large differences in the quantities of healing agent in the surrounding cementitious matrix. This is due to the fact that the viscosity of the 2:1 and 1:1 formulations is much lower and the curing time is much slower (and therefore the rate of increase of viscosity), leading to a much higher quantity of healing agent flowing into the cementitious matrix surrounding the crack.

The model parameters used in the simulations can be seen in Table 5.

In order to use the model predictively, it is necessary to know how the healing agent properties change with the different formulations. In the present work, different formulations relate to different quantities of AA incorporated and as such, it was decided to develop relationships for the healing agent properties as a function of the fraction of AA. For the viscosity, we employ Equation (1), whilst for the contact angle and healing time parameter we propose the following two relationships:

$$\theta = \begin{cases} a_1 - a_2 \tanh\left(\dfrac{\varphi_{AA} - a_3}{a_4}\right), \forall \varphi_{AA} \leq b \\ a_5 - a_6 \tanh\left(\dfrac{\varphi_{AA} - a_7}{a_8}\right), \forall \varphi_{AA} > b \end{cases} \tag{21a}$$

Table 4
Predicted healing agent quantities.

	Mass of n-CA formulation (g)		
Location	CA	2:1	1:1
Matrix	0.25	16.62	21.68
Crack	1.53	1.37	1.39
Total	1.79	17.99	23.07

Table 5
Model parameters.

Parameter	Value	Parameter	Value
E, E_h (N/mm^2)	30,000	m (−)	0.44
v, v_h (−)	0.2	λ (−)	−3
f_t (N/mm^2)	2.9	ρ (kg/m^3)	1060
d_m (mm)	0.25	φ_g (−)	1
f_{th} (N/mm^2)	3.4	nv (−)	2.193
d_{mh} (mm)	0.13	γ (N/m)	0.033
z_{c0} (mm)	0.2	c_{a1} (−)	1.325
z_{c1} (mm)	45	c_{a2} (−)	0.35
K_{mi} (m^2)	3×10^{-15}	β_w (m^3/Ns)	0.005
a (N/mm^2)	18,620,000		

$$\tau = \left(c_1 \varphi_{AA}^2 - c_2 \varphi_{AA} + c_3\right)\left(\frac{1}{1 - \varphi_{AA}}\right) \tag{22}$$

where the parameters a_i, b and c_i are constants to be calibrated.

The contact angle relationship was calibrated using experimental measurements for different formulations, whilst the healing time parameter relationship was determined using the values employed in the three-point bending tests, accounting for the fact that at an AA fraction of 1, no healing would occur. The fit of these equations to the data points can be seen in Fig. 7 and the constants are given in Table 6.

The error bars in Fig. 7a) relate to the uncertainty in the experimentally measured values of the contact angle (see Table 2). It is noted that such error bars are not seen in Fig. 7b) as the healing time parameter is a fitted numerical parameter from a deterministic model (i. e. we do not account for uncertainty in its value).
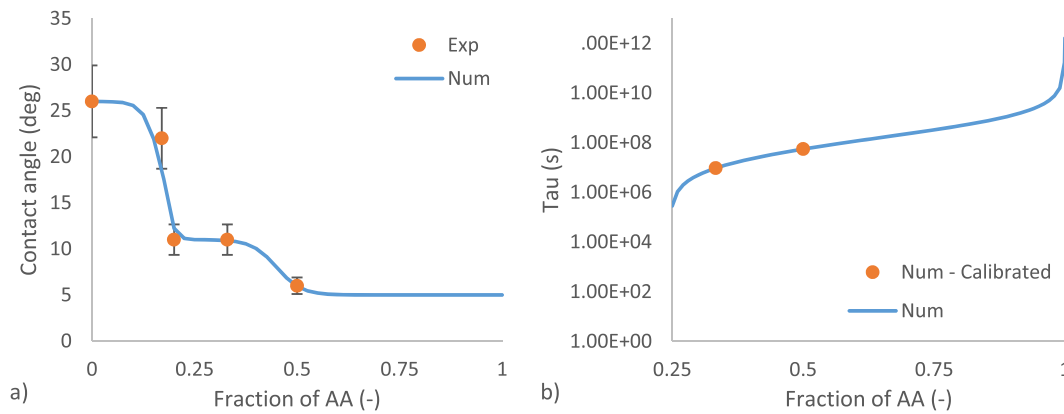
Fig. 7. Healing agent parameters and relationships a) contact angle and b) healing time parameter.

Table 6
Calibrated constants for wettability and healing time relationships.

Parameter	Value	Parameter	Value
a_1 (deg)	18.5	a_7 (−)	0.45
a_2 (deg)	7.5	a_8 (−)	0.06
a_3 (−)	0.17	b (−)	0.2
a_4 (−)	0.04	c_1 (s)	2.16×10^8
a_5 (deg)	8	c_2 (s)	5.33×10^7
a_6 (deg)	3	c_3 (s)	60

4.4. Predictive simulations and design curves

Following the calibration of the numerical model, it was decided to undertake a set of predictive simulations to illustrate how the model may be used to guide the development of self-healing materials, as well as aid the selection of healing agents. To this end, a number of different cases were considered, and design curves were produced based on the results. An example of this can be seen in Fig. 8 that shows how the time to reach a given degree of healing (in this case 80%) depends on both the width of the crack to be healed, and the healing time parameter, with the latter being dependent on the healing agent formulation. Thus, for a given crack width and healing time, the appropriate healing agent may be determined.

In addition to the healing time, the volume of healing agent required and the time taken to fill cracks were also considered. A number of different cases were simulated which considered the effects on the healing processes of varying the crack width, viscosity, applied pressure to the vascular network and crack length. A summary of the cases considered is given in Table 7.

The results can be seen in Figs. 9 and 10 for the healing agent volumes and Fig. 11 for the time taken to fill cracks of different widths and

lengths. For the healing agent volumes, it can be seen that there is a linear dependence on the viscosity of the healing agent, with more viscous agents requiring lower volumes due to the reduction in the transport (or loss) of agent into the surrounding cementitious matrix. The application of an applied pressure increases the volume of healing agent required. This is due to the increase in the transport into the surrounding cementitious matrix and can clearly be seen in Fig. 10 for the case of 0.02 N/m² viscosity.

The crack filling time results show that there is a strong dependence on the applied pressure, with large jumps in times observed as soon as any pressure is applied. For a 75 mm crack, the application of a pressure of just 0.1 bar results in an 82 fold decrease in the crack filling time. For both the crack length, and crack width, there is a much more modest dependence, with up to a 16 fold increase observed when increasing crack length, and up to a 10 fold increase when reducing crack width. In all cases, the viscosity dependence is complex, with the highest filling times not necessarily being associated with the highest viscosities. This is due to the complex interplay between the physical processes; the viscosity increases the viscous resistance that reduces flow rate, but reduces the flow into the surrounding cementitious matrix that increases flow rate. It is also interesting to note that reducing the crack width reduces the time taken to fill cracks when no additional pressure is applied, whilst the opposite is true when an additional pressure is applied. This again, is due to the complex interaction between the physical processes. Whilst reducing the crack width reduces the crack permeability, it also increases the capillary pressure that drives the flow. When there is an additional applied pressure, the effect of the capillary pressure is reduced and therefore the crack permeability has a larger role in the difference between the filling times for the two crack widths.

The examples presented in this subsection illustrate the predictive capability of the numerical model and its potential as a tool for guiding the development of and/or aiding the selection of novel healing agents. It is recognised that the development of a comprehensive set of design curves would require many more cases to be considered. In addition, the production of such a set of design curves may be hindered by the dependence of the response on a large number of factors. As such, it may be challenging to represent the results and dependencies graphically; for example, each graph in Fig. 10 relates to a single crack width and length and shows dependence on viscosity and pressure, as opposed to showing all dependencies. A promising alternative approach would be to use machine learning. Machine learning models could be trained on model results, and used as 'surrogate' models for guiding the development/ aiding the selection of novel healing agents through the prediction of the response for a given scenario and varying healing agent properties. Such an approach is the subject of ongoing research.
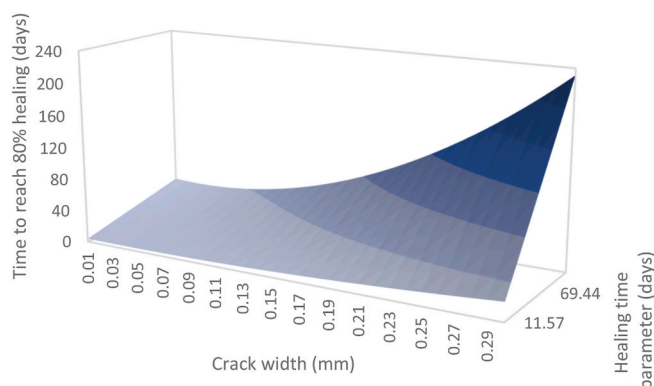

Fig. 8. Predicted healing time.

Table 7
Cases considered (repeated for two crack lengths, 37.5 mm and 75 mm).

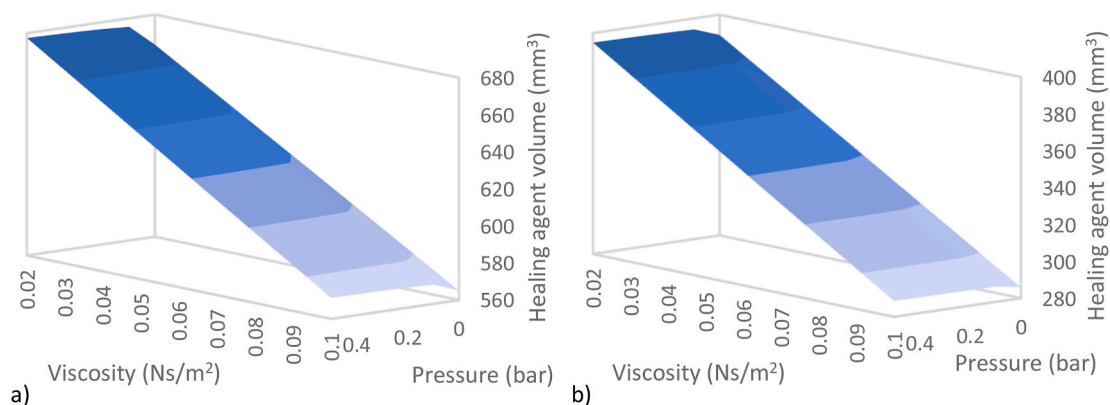| Case	Crack Width (mm)	Viscosity (Ns/m^2)	Applied Pressure (Bar)	Case	Crack Width (mm)	Viscosity (Ns/m^2)	Applied Pressure (Bar)
1	0.1	0.0781	0	10	0.05	0.0781	0
2	0.1	0.0781	0.1	11	0.05	0.0781	0.1
3	0.1	0.0781	0.3	12	0.05	0.0781	0.3
4	0.1	0.0585	0	13	0.05	0.0585	0
5	0.1	0.0585	0.1	14	0.05	0.0585	0.1
6	0.1	0.0585	0.3	15	0.05	0.0585	0.3
7	0.1	0.031	0	16	0.05	0.031	0
8	0.1	0.031	0.1	17	0.05	0.031	0.1
9	0.1	0.031	0.3	18	0.05	0.031	0.3

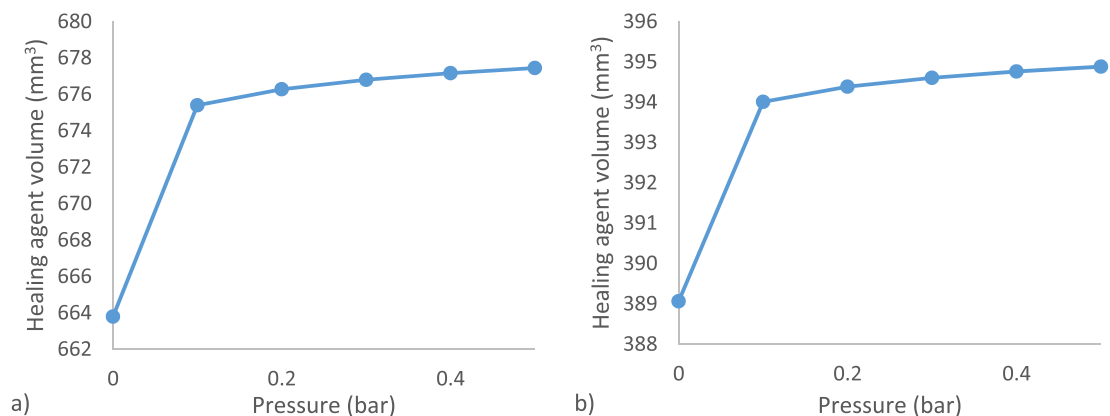**Fig. 9.** Predicted healing agent volumes for a) 0.1 mm crack and b) 0.05 mm crack.

Fig. 10. Predicted healing agent volumes for 0.02 N/m^2 viscosity agent and a) 0.1 mm crack and b) 0.05 mm crack.

4.5. Predictive simulation and physical test of 'ideal' healing agent

In order to test the predictive capability of the model a three-point bending test of concrete samples containing vascular networks, presented in section 2.4, was considered. The model was used to predict the response of different formulations, not yet tested physically, and the 'ideal' healing agent for this application selected. The 'ideal' healing agent identified corresponded to a 3:1 formulation. Following this selection, a 3:1 formulation was prepared before being physically tested in the laboratory, to see how accurate the blind model predictions were. The experimental and numerical results are given in Fig. 12. This shows that the model predictions accurately capture the average response. It is noted that there is significant variability in the experimental results, particularly in the stage 3 response. For completeness, the predicted healing agent quantity used is shown in Table 8. The accuracy of the predictions indicate that the numerical model is a reliable tool that can be used to guide the development of, and analyse, self-healing

cementitious materials utilising novel healing agents.

5. Conclusions and final remarks

In this study, a combined experimental-numerical testing programme for the development of novel healing agents for use in self-healing cementitious materials has been presented. Based upon the results of this study, the following conclusions have been drawn.

- The addition of acrylic acid is an effective means of tailoring the chemo-rheological properties of cyanoacrylate based healing agents.
- The novel cyanoacrylate formulations are effective healing agents for self-healing cementitious materials, having suitable chemo-rheological properties, and lead to a good recovery of mechanical properties when employed in a vascular self-healing system.
- Tailoring novel healing agents can lead to a notable improvement in their performance, as shown by the results of the 3:1 formulation that
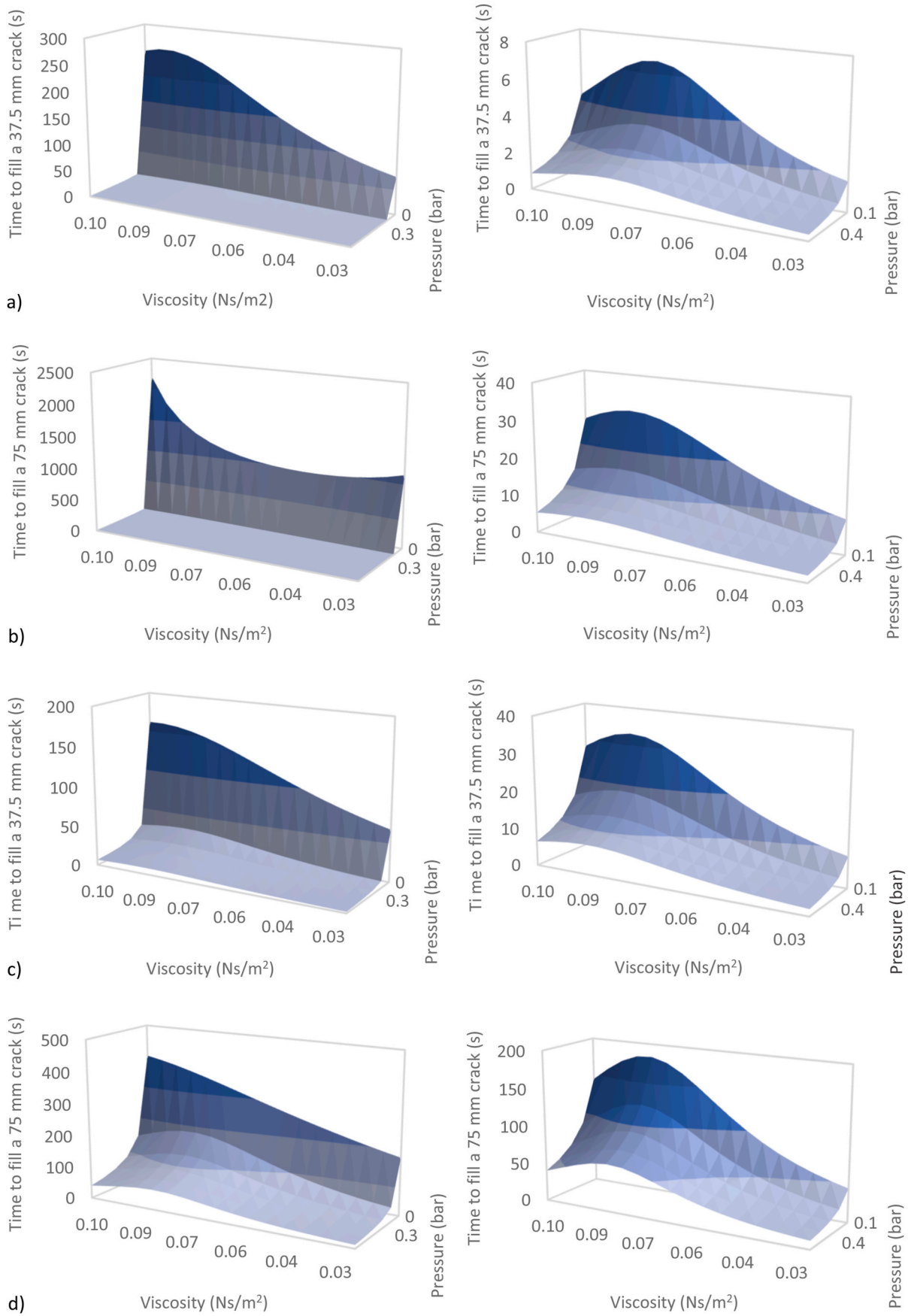
Fig. 11. Predicted time to fill cracks of a) 0.1 mm width, 37.5 mm length, b) 0.1 mm width, 75 mm length, c) 0.05 mm width, 37.5 mm length and d) 0.05 mm width, 75 mm length. The graphs on the left show the full set of results, whilst the graphs on the right show the range of pressures 0.1–0.5 bar.
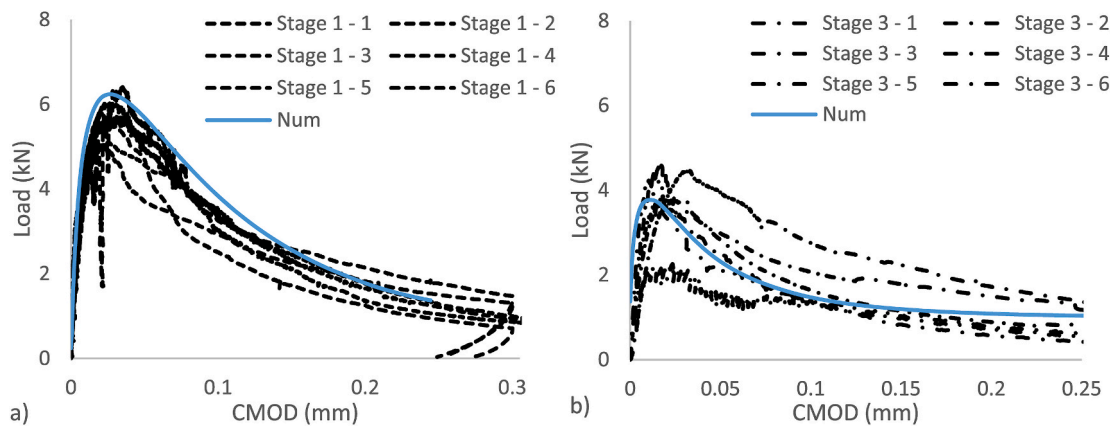
Fig. 12. Mechanical response of 3:1 formulation a) stage 1 and b) stage 3.

Table 8
Predicted healing agent quantity.

Location	Mass of n-CA formulation (g)
	3:1
Matrix	14.94
Crack	1.37
Total	16.30

yielded an increase in strength recovery of 48% when compared to the best performing original formulation (2:1) and 24% when compared to a commercial cyanoacrylate.

- The numerical model is able to accurately reproduce experimental three-point bend test data for self-healing cementitious materials employing novel healing agents.
- The development of the numerical model alongside a detailed experimental study provides insight into the underlying physical processes and results in a model with good predictive capability.
- A combined experimental-numerical study, consisting of physical tests, calibration of model parameters and the production of design curves, is an effective means of developing novel materials.

Author contributions

Conceptualization, C.dN, BLF.; Methodology, CdN, BLF T.J, ; Writing—original draft preparation, C. dN, BLF; Writing—review and editing, D. G, T.J. C.dN. BLF; Supervision, T.J. and D.G.; Project administration, T.J.; Funding acquisition, T.J. and D.G.

Declaration of competing interest

The authors declare the following financial interests/personal relationships which may be considered as potential competing interests: Cristina De Nardi reports financial support was provided by Engineering and Physical Sciences Research Council. Brubeck Lee Freeman reports financial support was provided by Engineering and Physical Sciences Research Council. Diane Gardner reports financial support was provided by Engineering and Physical Sciences Research Council. Antony Jefferson reports financial support was provided by Engineering and Physical Sciences Research Council.

Data availability

The link to my data will be reported by the time of publication. Information on the data underpinning the results presented here, including how to access them, can be found in the Cardiff University data catalogue at (http://doi.org/10.17035/d.2023.0259875526).

References

[1] B. Blaiszik, S. Kramer, S. Olugebefola, J. Moore, N. Sottos, Self-healing polymers and composites, Annu. Rev. Mater. Res. 40 (2010) 179–211211, https://doi.org/10.1146/annurev-matsci-070909-104532.

[2] C. Dry, Matrix cracking repair and filling using active and passive modes for smart timed release of chemicals from fibers into cement matrices, Smart Mater. Struct. 3 (2) (Jun. 1994) 118–123, https://doi.org/10.1088/0964-1726/3/2/006.

[3] E. Tsangouri, et al., Feasibility study on real-scale, self-healing concrete slab by developing a smart capsules network and assessed by a plethora of advanced monitoring techniques, Construct. Build. Mater. 228 (2019), 116780, https://doi.org/10.1016/j.conbuildmat.2019.116780.

[4] P. Minnebo, et al., A novel design of autonomously healed concrete: towards a vascular healing network, Materials 10 (1) (2017) 1–23, https://doi.org/10.3390/ma10010049.

[5] C. Xue, W. Li, A. Castel, K. Wang, D. Sheng, Effect of incompatibility between healing agent and cement matrix on self-healing performance of intelligent cementitious composite, Smart Mater. Struct. 29 (11) (2020), https://doi.org/10.1088/1361-665X/aba9ac.

[6] R. Davies, T. Jefferson, D. Gardner, Development and testing of vascular networks for self-healing cementitious materials, J. Mater. Civ. Eng. 33 (7) (Jul. 2021), 4021164, https://doi.org/10.1061/(ASCE)MT.1943-5533.0003802.

[7] Z. Li, L.R. De Souza, C. Litina, A.E. Markaki, A. Al-Tabbaa, A novel biomimetic design of a 3D vascular structure for self-healing in cementitious materials using Murray's law, Mater. Des. 190 (2020) 1–14, https://doi.org/10.1016/j.matdes.2020.108572.

[8] C. De Nardi, D. Gardner, A.D. Jefferson, Development of 3D printed networks in self-healing concrete, Materials 13 (6) (Mar. 2020) 1328, https://doi.org/10.3390/ma13061328.

[9] Y. Shields, N. De Belie, A. Jefferson, K. Van Tittelboom, A review of vascular networks for self-healing applications, Smart Mater. Struct. 30 (6) (2021), https://doi.org/10.1088/1361-665X/abf41d.

[10] Z. Wan, Y. Xu, Y. Zhang, S. He, B. Šavija, Mechanical properties and healing efficiency of 3D-printed ABS vascular based self-healing cementitious composite: experiments and modelling, Eng. Fract. Mech. 267 (2022), 108471, https://doi.org/10.1016/j.engfracmech.2022.108471.

[11] V.C. Li, Y.M. Lim, Y.W. Chan, Feasibility study of a passive smart self-healing cementitious composite, Compos. B Eng. 29 (6) (1998) 819–827, https://doi.org/10.1016/S1359-8368(98)00034-1.

[12] K. Van Tittelboom, Self-Healing Concrete through Incorporation of Encapsulated Bacteria- or Polymer-Based Healing Agents ('Zelfhelend Beton Door Incorporatie Van Ingekapselde Bacteri, UGent, 2012.

[13] K. Van Tittelboom, N. De Belie, D. Van Loo, P. Jacobs, Self-healing efficiency of cementitious materials containing tubular capsules filled with healing agent, Cem. Concr. Compos. 33 (4) (2011) 497–505, https://doi.org/10.1016/j.cemconcomp.2011.01.004.

[14] A. Jefferson, C. Joseph, R. Lark, B. Isaacs, S. Dunn, B. Weager, A new system for crack closure of cementitious materials using shrinkable polymers, Cement Concr. Res. 40 (5) (2010) 795–801, https://doi.org/10.1016/j.cemconres.2010.01.004.

[15] C. Joseph, D. Gardner, T. Jefferson, B. Isaacs, B. Lark, Self-healing cementitious materials: a review of recent work, Proc. Inst. Civ. Eng. - Constr. Mater. 164 (1) (2011) 29–41, https://doi.org/10.1680/coma.900051.

[16] L. Sun, W.Y. Yu, Q. Ge, Q.G. Ling Sun, Yong Yu Wen, Experimental research on the self-healing performance of micro-cracks in concrete bridge, Adv. Mater. Res. 250–253 (2011) 28–32. https://doi.org/10.4028/www.scientific.net/AMR.250-253.28.

[17] R. Davies, D. Gardner, J. Anthony, B. Lark, A novel 2d vascular network in cementitious materials, in: FIB Proceedings - Concrete – Innovation and Design, FIB - Féd. Int. du Béton, Copenhagen, 2015.

[18] T. Selvarajoo, R.E. Davies, B.L. Freeman, A.D. Jefferson, Mechanical response of a vascular self-healing cementitious material system under varying loading conditions, Construct. Build. Mater. 254 (2020), 119245, https://doi.org/10.1016/j.conbuildmat.2020.119245.

[19] P. Klemarczyk, J. Guthrie, 5 - advances in anaerobic and cyanoacrylate adhesives, in: D.A.B. T.-A, S.A.B. Dillard (Eds.), Woodhead Publishing Series In Welding And Other Joining Technologies, Woodhead Publishing, 2010, pp. 96–131.

[20] M. J. Tomlinson, A. Tomlinson, M. L. Chapman, A. D. Jefferson, and H. D. Wright, 'Shell composite construction for shallow draft immersed tube tunnels', in Immersed tunnel techniques, pp. 209–220.

[21] D. Gardner, A. Jefferson, A. Hoffman, Investigation of capillary flow in discrete cracks in cementitious materials, Cement Concr. Res. 42 (7) (2012) 972–981, https://doi.org/10.1016/j.cemconres.2012.03.017.

[22] C. Joseph, A.D. Jefferson, M.B. Cantoni, Issues relating to the autonomic healing of cementitious materials, First Int. Conf. Self Heal. Mater. (April) (2007) 1–8.

[23] C. De Nardi, et al., Experimental investigation of a novel formulation of a cyanoacrylate-based adhesive for self-healing concrete technologies, Front. Built Environ. 7 (June) (2021) 1–15, https://doi.org/10.3389/fbuil.2021.660562.

[24] T. Jefferson, E. Javierre, B. Freeman, A. Zaoui, E. Koenders, L. Ferrara, Research progress on numerical models for self-healing cementitious materials, Adv. Mater. Interfac. 5 (17) (2018) 1–19, https://doi.org/10.1002/admi.201701378.

[25] N. De Belie, K. Van Tittelboom, M. Sánchez Moreno, L. Ferrara, E. Gruyaert, Self-Healing Concrete Research in the European Projects SARCOS and SMARTINCS BT - Proceedings of the 3rd RILEM Spring Convention and Conference, RSCC 2020, 2022, pp. 303–307.

[26] C. De Nardi, D. Gardner, D. Cristofori, L. Ronchin, A. Vavasori, T, Jefferson, Advanced 3D printed mini-vascular network for self-healing concrete, Mater. Des. 230 (2023), 111939, https://doi.org/10.1016/j.matdes.2023.111939.

[27] G.Z. Voyiadjis, P.I. Kattan, Healing and super healing in continuum damage mechanics, Int. J. Damage Mech. 23 (2) (2014) 245–260, https://doi.org/10.1177/1056789513491773.

[28] G.A. Esgandani, A. El-Zein, Thermodynamic based model for coupled elastoplastic damage-healing behaviour of unsaturated geomaterials, Mech. Mater. 145 (2020), 103395, https://doi.org/10.1016/j.mechmat.2020.103395.

[29] R. Davies, A. Jefferson, Micromechanical modelling of self-healing cementitious materials, Int. J. Solid Struct. 113 (114) (2017) 180–191, https://doi.org/10.1016/j.ijsolstr.2017.02.008.

[30] S. Zhou, H. Zhu, J.W. Ju, Z. Yan, Q. Chen, Modeling microcapsule-enabled self-healing cementitious composite materials using discrete element method, Int. J. Damage Mech. 26 (2) (2017) 340–357, https://doi.org/10.1177/1056789516688835.

[31] F.A. Gilabert, D. Garoz, W. Van Paepegem, Macro- and micro-modeling of crack propagation in encapsulation-based self-healing materials: application of XFEM and cohesive surface techniques, Mater. Des. 130 (2017) 459–478, https://doi.org/10.1016/j.matdes.2017.05.050.

[32] Y. Zhang, X. Zhuang, A softening-healing law for self-healing quasi-brittle materials: analyzing with strong discontinuity embedded approach, Eng. Fract. Mech. 192 (2018) 290–306, https://doi.org/10.1016/j.engfracmech.2017.12.018.

[33] B.L. Freeman, P. Bonilla-Villalba, I.C. Mihai, W.F. Alnaas, A.D. Jefferson, A specialised finite element for simulating self-healing quasi-brittle materials, Adv. Model. Simul. Eng. Sci. 7 (1) (2020) 32, https://doi.org/10.1186/s40323-020-00171-4.

[34] A. Aliko-Benítez, M. Doblaré, J.A. Sanz-Herrera, Chemical-diffusive modeling of the self-healing behavior in concrete, Int. J. Solid Struct. 69 (70) (2015) 392–402, https://doi.org/10.1016/j.ijsolstr.2015.05.011.

[35] A.S. Chitez, A.D. Jefferson, A coupled thermo-hygro-chemical model for characterising autogenous healing in ordinary cementitious materials, Cement Concr. Res. 88 (2016) 184–197, https://doi.org/10.1016/j.cemconres.2016.07.002.

[36] B.L. Freeman, T. Jefferson, The simulation of transport processes in cementitious materials with embedded healing systems, Int. J. Numer. Anal. Methods GeoMech. 44 (2) (Feb. 2020) 293–326, https://doi.org/10.1002/nag.3017.

[37] F.A. Gilabert, K. Van Tittelboom, J. Van Stappen, V. Cnudde, N. De Belie, W. Van Paepegem, Integral procedure to assess crack filling and mechanical contribution

[38] of polymer-based healing agent in encapsulation-based self-healing concrete, Cem. Concr. Compos. 77 (2017) 68–80, https://doi.org/10.1016/j.cemconcomp.2016.12.001.

[38] H. Huang, G. Ye, Simulation of self-healing by further hydration in cementitious materials, Cem. Concr. Compos. 34 (4) (2012) 460–467, https://doi.org/10.1016/j.cemconcomp.2012.01.003.

[39] H.A.A. Algaifi, S.A. Bakar, A.R.M. Sam, A.R.Z. Abidin, S. Shahir, W.A.H. Altowayti, Numerical modeling for crack self-healing concrete by microbial calcium carbonate, Construct. Build. Mater. 189 (2018) 816–824, https://doi.org/10.1016/j.conbuildmat.2018.08.218.

[40] G. Di Luzio, L. Ferrara, V. Krelani, Numerical modeling of mechanical regain due to self-healing in cement based composites, Cem. Concr. Compos. 86 (2018) 190–205, https://doi.org/10.1016/j.cemconcomp.2017.11.006.

[41] J.A. Sanz-Herrera, A. Aliko-Benitez, A.M. Fadrique-Contreras, Numerical investigation of the coupled mechanical behavior of self-healing materials under cyclic loading, Int. J. Solid Struct. 160 (2019) 232–246, https://doi.org/10.1016/j.ijsolstr.2018.10.029.

[42] C.R. Rodríguez, S.C. Figueiredo, M. Deprez, D. Snoeck, E. Schlangen, B. Šavija, Numerical investigation of crack self-sealing in cement-based composites with superabsorbent polymers, Cem. Concr. Compos. 104 (2019), 103395, https://doi.org/10.1016/j.cemconcomp.2019.103395.

[43] A. Cibelli, M. Pathirage, G. Cusatis, L. Ferrara, G. Di Luzio, A discrete numerical model for the effects of crack healing on the behaviour of ordinary plain concrete: implementation, calibration, and validation, Eng. Fract. Mech. 263 (2022), 108266, https://doi.org/10.1016/j.engfracmech.2022.108266.

[44] A.D. Jefferson, B.L. Freeman, A crack-opening-dependent numerical model for self-healing cementitious materials, Int. J. Solid Struct. 244 (245) (2022), 111601, https://doi.org/10.1016/j.ijsolstr.2022.111601.

[45] B. Hilloulin, D. Hilloulin, F. Grondin, A. Loukili, N. De Belie, Mechanical regains due to self-healing in cementitious materials: experimental measurements and micro-mechanical model, Cement Concr. Res. 80 (2016) 21–32, https://doi.org/10.1016/j.cemconres.2015.11.005.

[46] G. Cusatis, D. Pelessone, A. Mencarelli, Lattice discrete particle model (LDPM) for failure behavior of concrete. I: theory, Cem. Concr. Compos. 33 (9) (2011) 881–890, https://doi.org/10.1016/j.cemconcomp.2011.02.011.

[47] T. Selvarajoo, R.E. Davies, D.R. Gardner, B.L. Freeman, A.D. Jefferson, Characterisation of a vascular self-healing cementitious material system: flow and curing properties, Construct. Build. Mater. 245 (2020), 118332, https://doi.org/10.1016/j.conbuildmat.2020.118332.

[48] A.S. Teja, P. Rice, Generalized corresponding states method for the viscosities of liquid mixtures, Ind. Eng. Chem. Fundam. 20 (1) (1981) 77–81, https://doi.org/10.1021/i100001a015.

[49] R. Davies, et al., Large scale application of self-healing concrete: design, construction, and testing, Front. Mater. 5 (2018) 51, https://doi.org/10.3389/fmats.2018.00051.

[50] C. Joseph, A.D. Jefferson, B. Isaacs, R. Lark, D. Gardner, Experimental investigation of adhesive-based self-healing of cementitious materials, Mag. Concr. Res. 62 (11) (2010) 831–843, https://doi.org/10.1680/macr.2010.62.11.831.

[51] F.P. Robertson, L.J. Magill, C. Davidson, H. Mitchell, B.R. Davidson, 8 - Cyanoacrylate Tissue Glues for Cutaneous Wound Closure, vol. 2, Elsevier Ltd, 2016.

[52] W. M. . Kosmatka S. H, Design and Control of Concrete Mixtures, fifteenth ed. (Washington DC).

[53] British Standard, BS EN 12390-5:2019 BS EN 12390-5:2019 Testing Hardened Concrete, 2019. Brussels.

[54] European Standard, EN 1992-1-1 Eurocode 2: Design of Concrete Structures - Part 1-1 : General Rules and Rules for Buildings, 2011. Brussels.

[55] L. Li, S.H. Lee, Efficient field-scale simulation of black oil in a naturally fractured reservoir through discrete fracture networks and homogenized media, SPE Reservoir Eval. Eng. 11 (4) (2008) 750–758.

[56] J.M. Castro, C.W. Macosko, Kinetics and rheology of typical polyurethane reaction injection molding systems, Soc. Plast. Eng. (Technical Pap. (1980) 434–438.

[57] D. Homma, H. Mihashi, T. Nishiwaki, Self-healing capability of fibre reinforced cementitious composites, J. Adv. Concr. Technol. 7 (2) (2009) 217–228, https://doi.org/10.3151/jact.7.217.

[58] L. Ferrara, V. Krelani, Engineering Self Healing capacity of cement based materials through crystalline admixtures, in: ICSHM2015 International Conference on Self-Healing Materials, 2015, pp. 1–4.

[59] G.L. Schneberger, Adhesive bonding, Adhes. Age 23 (1) (1980) 42–46.